A non-linear mathematical model for the X-ray variability of the microquasar GRS 1915+105 - III: Low-frequency Quasi Periodic Oscillations

E. Massaro[1], F. Capitanio[1]*, M. Feroci[1]*, T. Mineo[2]*

[1] *INAF, IAPS, via del Fosso del Cavaliere 100, I-00113 Roma, Italy*
[2] *INAF, IASF Palermo, via U. La Malfa 153, I-90146 Palermo, Italy*

VERSIONE 3.2   Roma 23 Giugno 2020

ABSTRACT
The X-ray emission from the microquasar GRS 1915+105 shows, together with a very complex variability on different time scales, the presence of low-frequency quasi periodic oscillations (LFQPO) at frequencies lower than ∼30 Hz. In this paper, we demonstrate that these oscillations can be consistently and naturally obtained as solutions of a system of two ordinary differential equations that is able to reproduce almost all variability classes of GRS 1915+105. We modified the Hindmarsh-Rose model and obtained a system with two dynamical variables $x(t)$, $y(t)$, where the first one represents the X-ray flux from the source, and an input function $J(t)$, whose mean level J_0 and its time evolution is responsible of the variability class. We found that for values of J_0 around the boundary between the unstable and the stable interval, where the equilibrium points are of spiral type, one obtain an oscillating behaviour in the model light curve similar to the observed ones with a broad Lorentzian feature in the power density spectrum and, occasionally, with one or two harmonics. Rapid fluctuations of $J(t)$, as those originating from turbulence, stabilize the low-frequency quasi periodic oscillations resulting in a slowly amplitude modulated pattern. To validate the model we compared the results with real *RXTE* data which resulted remarkably similar to those obtained from the mathematical model. Our results allow us to favour an intrinsic hypothesis on the origin of LFQPOs in accretion discs ultimately related to the same mechanism responsible for the spiking limit cycle.

Key words: black hole physics âĂŞ binaries: close âĂŞ stars: individual: GRS 1915+105 âĂŞ X-rays:stars.

1 INTRODUCTION

Quasi Periodic Oscillations (QPO) in X-ray binaries were discovered in the eighties (van der Klis 1989) and they were after detected in several Black Hole candidates (BHC) (Remillard & McClintock 2006). Low-Frequency QPOs (LFQPO) are observed as broad peaks with a well approximate Lorentzian profiles in the Power Spectral Density (PDS) and centered at a frequency $\nu_0 \lesssim 30$ Hz (see the review by Motta 2016). LFQPOs have been classified in different types (Wijnands et al. 1999; Remillard & McClintock 2006; Casella et al. 2004, 2005; Motta 2016) according to the peak frequency and width, the relevance of the harmonics and the shape of the noise in the PDS. Many obser-

vational studies have shown that central frequencies vary and exhibit correlations with the mean brightness and with the energy of the photons. Following van den Eijnden et al. (2016) one can classify the explanations of LFQPOs into the broad types of *geometric* and *intrinsic* models: In the former class, the source luminosity is not time modulated but has an anisotropic angular pattern and the flux oscillations are produced by changes of orientation with respect to the of sight line (e.g. precession or Lense-Thirring effect as proposed by Ingram et al. (2009)), while in the latter type, the QPO origin is related to emissivity changes due to shocks (Chakrabarti & Molteni 1993), or variations of the accretion rate originated in various kinds of instabilities (Chen & Taam 1992, 1995; Tagger & Pellat 1999; Varnière et al. 2012; Marcel et al. 2020).

In the present paper we consider the well studied microquasar GRS 1915+105, discovered by Castro-Tirado et al.

---

* E-mail:fiamma.capitanio@inaf.it (FC);
marco.feroci@inaf.it (MF); teresa.mineo@inaf.it (TM)
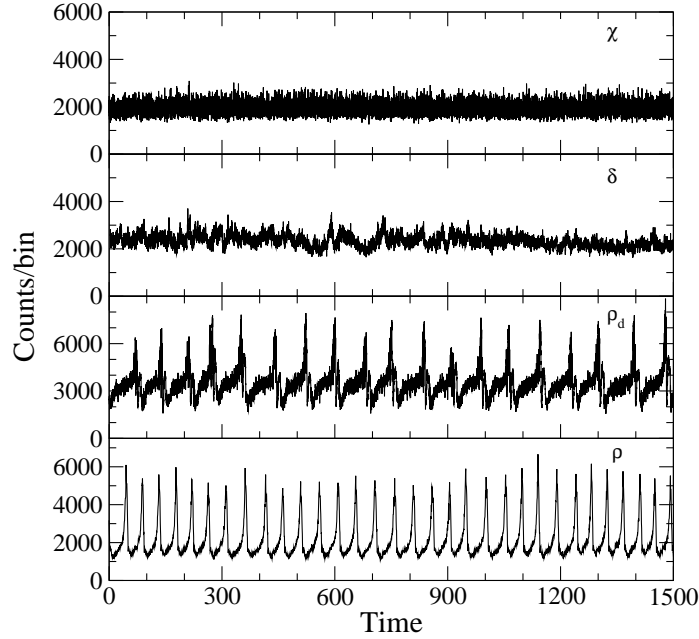
Figure 1. Examples of four types of *RXTE* light curves of GRS 1915+105. The greek letters correspond to the variability classes according to the definition by Belloni et al. (2000).
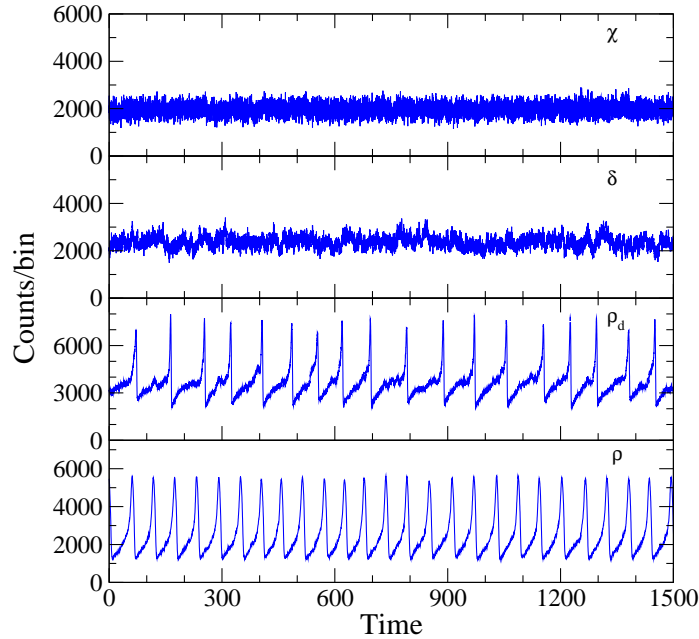
Figure 2. Solutions of the mathematical model described by Paper I and Paper II and reproducing the observed light curves GRS 1915+105 in Fig. 1. These series, from top to bottom, are obtained by increasing only a parameter as explained in Sect. 3.

(1992). This source exhibits a bright and highly variable X-ray emission, characterized by several different variability patterns, that alternate steady and noisy emission to regular and chaotic series of bursts. A first classification of the observed multifarious time behavior based on the signal

structure and on the photon energy distribution was presented by Belloni et al. (2000), who defined twelve classes identified by a greek letter, but new other patterns were observed on subsequent occasions. Some examples of X-ray light curves, from the *RXTE* data archive of four of these

variability classes are shown in Fig. 1. In the top panel there is a typical χ class light curve that consists of a rather steady and highly noisy signal with a nearly constant mean value, and in the bottom panel there is a ρ class light curve with a long sequence of nearly regular bursts. In the two intermediate panels there are examples of δ and ρ_d signals, the latter defined by Massaro et al. (2020a), that are considered transition classes between stable and unstable states. A bursting ρ class light curve was first reported by Taam et al. (1997), who interpreted it as an evidence of a limit cycle in an accretion disc around a black hole originating from thermal-viscous instabilities (see also Taam & Lin 1984; Szuszkiewicz & Miller 1998).

LFQPOs are frequently observed also in GRS 1915+105 (Paul et al. 1997; Fender & Belloni 2004). Markwardt et al. (1999) and Muno et al. (1999) found that these oscillations occur during the dips, when the source is in a flaring state, and that their frequency correlates with the parameters of the thermal disc component, like the temperature. Rodriguez et al. (2002) confirmed that frequency variations are well correlated with the soft X-ray flux and proposed that they could be related to a hot point in an optically thick disc, while the presence of harmonics could be a signature of a non-linear instability. The high X-ray flux from GRS 1915+105 allows for detailed investigations on LFQPOs which showed the existence of a modulation with the QPO phase either of the observed reflection fraction or of the iron line shape that change throughout the cycle (Ingram & van der Klis 2015).

The stability of accretion discs is also a very interesting subject of investigations since many years and theoretical analysis suggested that thermal and viscous instabilities can develop and establish a limit cycle behavior. The complex hydrodynamical, thermal and magnetic phenomena occurring in accretion discs around black holes involve non-linear processes whose evolution are described by a system of partial differential equations, whose solutions are obtained by numerical calculations involving several quantities not directly observable, as the gas density or viscous stresses.

In a recent couple of papers, (Massaro et al. 2020a,b, hereafter Paper I and Paper II), we showed that the solutions of a system of non-linear ordinary differential equations (ODE) reproduce several classes of the X-ray light curves of GRS 1915+105. This system, named Modified Hindmarsh-Rose (shortly MHR), is a modified version of the well studied Hindmarsh-Rose model that is used for describing neuronal bursts. MHR model is a non-autonomous system with a time dependent input function. The function we adopted has a variable component added to fast random fluctuations introduced to simulate a possible plasma turbulence in the emitting source. Some examples of the numerical solutions obtained in Paper I are given in Fig. 2. These light curves, remarkably similar to the true data in Fig. 1, are obtained by changing the value of only one parameter. It is interesting that the shape of one of the equilibrium curves of the proposed ODE system presents a S-pattern similar to those derived from numerical solutions of disc equations (see the review by Lasota (2016)). In stable states, like the χ class, that is much more frequently observed than all the other ones Belloni et al. (2000), the X-ray flux of GRS 1915+105 remains nearly constant, but a large noise component is present. This component may be particularly relevant

for reproducing some variability classes and can play a very important role in the origin of LFQPOs.

In the present paper we investigate in detail how the MHR model produces LFQPOs and how the amplitude of the noisy component affects the characteristics of the solutions. In particular, we present some results on LFQPOs in GRS 1915+105 applying a harmonic filtering method and, after a brief description of our mathematical model, we demonstrate that it can also account for LFQPOs with some features remarkably similar to the observed ones. These findings can be applied to other sources as well.
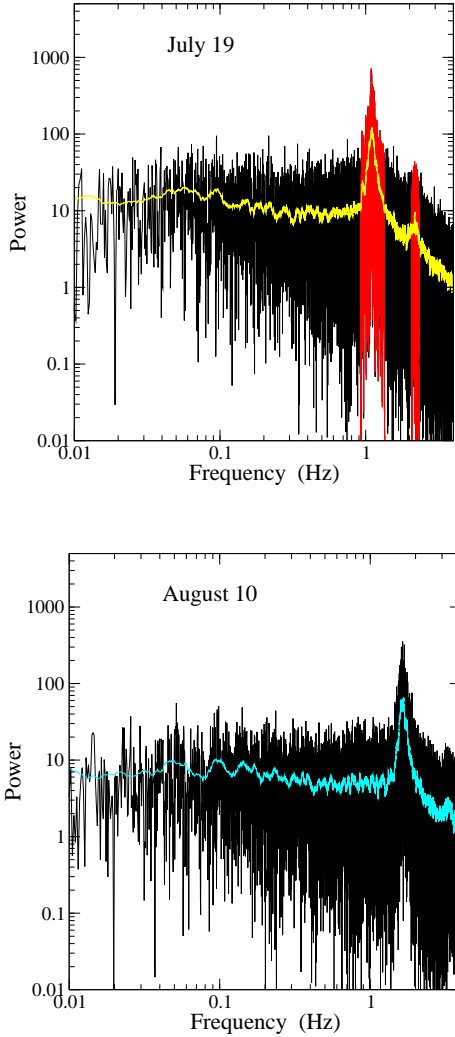
2 LFQPO ANALYSIS OF $RXTE$ OBSERVATIONS

Extensive investigations of several $RXTE$ observations of GRS 1915+105 focused on QPO detection and their properties were performed by Morgan et al. (1997) and Yan et al. (2013); more recently, van den Eijnden et al. (2016) reported new results on another sample of $RXTE$ data sets. We selected in these data a couple of observations having LFQPO features with high quality factors, and precisely those with ID 1040801-25-00 and 1040801-29-00a, both performed in 1996, the former on July 19 and the latter on August 10. The $RXTE$/PCA light curves were extracted in standard 1 mode, namely in the total energy band (2-40 keV) and with the time binning of 125 ms. Both observations include more than a single orbit and we selected only the first one to avoid time gaps in the data; then we computed their PDS by means of a standard Discrete Fourier transform algorithm. The July 19 series has a duration of 3296 s and that of August 10 of 2816 s.

In the two panels of Fig. 3, we report the PDS of both observations, whose values (black spectra) are affected by a very large noise that can be reduced by performing a simple running average smoothing; broad Lorentzian peaks centered at 1.11 Hz (July 19) and 1.66 Hz (August 10), in a very good agreement with the above quoted papers, are well apparent. Note that in both spectra a first harmonic feature is also present.

We reconstruct the time signal corresponding to these features applying a technique similar to that used by van den Eijnden et al. (2016) that consists in filtering both the real and imaginary series of the discrete Fourier transform of the photon count rates. We did not use the same optimal filter used by these authors but applied the simple rectangular bandpass with a smooth tapering at the boundaries given by the following formula:

$$
\Phi(X) = \frac{1}{4}\left(1 + \frac{(X - X_1)}{\sqrt{(X - X_1)^2 + s_1^2}}\right) \times
$$
$$
\left(1 - \frac{(X - X_2)}{\sqrt{(X - X_2)^2 + s_2^2}}\right) \quad (1)
$$

where X_1 and X_2 are the two frequencies defining the accepted window and s_1 and s_2 rules the slopes for tapering the filter profile (for a symmetric filter $s_1 = s_2$). In our case,
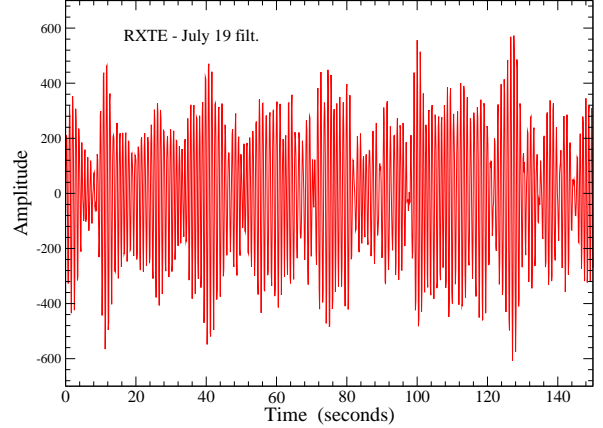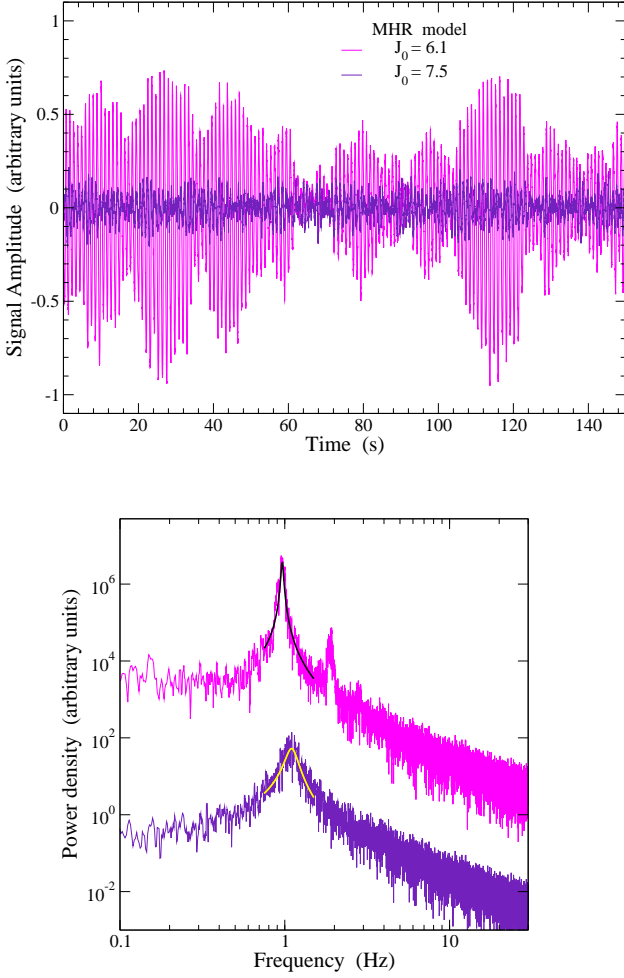
Figure 4. A short segment of the X-ray light curve of the *RXTE* observation of 1996 July 19 of GRS 1915+105 obtained by means of the two band Fourier filtering shown in the upper plot of Fig. 3.

in Fig. 2 is also able to produce LFQPOs with only a further increase of the input parameter and without any changes of the other parameters. In Fig. 5 we reported two series computed in the quoted paper and their PDS to show how the model gives LFQPOs remarkably similar to the true data. Light curves show a modulated fast oscillation with an amplitude depending on the input parameter. Note also the large differences in the amplitudes of these signals which are due to the values of J_0 but not to the amplitude of the noise, as explained in the next section. In the lower panel, the upper spectrum has a well apparent second harmonic and the third one is also marginally detectable, whereas in the lower spectrum only the peak at the fundamental frequency is visible. In the same plot we report the Lorentzian best fits to the peaks, which are in a very well agreement with their profiles and have quality factors $Q = \nu/\Delta\nu$ equal to 29.2 and 5.8, comparable to observed values.

Thus one can rise the hypothesis that the spikes of the limit cycle and LFQPO, both frequently observed in GRS 1915+105, have a common origin and their occurrence depends on the value of only one parameter. In the next section we summarize the main mathematical properties of the MHR model and extend the analysis of the nature of the equilibrium points in order to make clear the necessary conditions for developing LFQPOs. Moreover, the MHR model will make possible to investigate the relevant role of the presence of a noise component in stabilizing LFQPOs, which, in absence of such a component, would be rapidly damped.
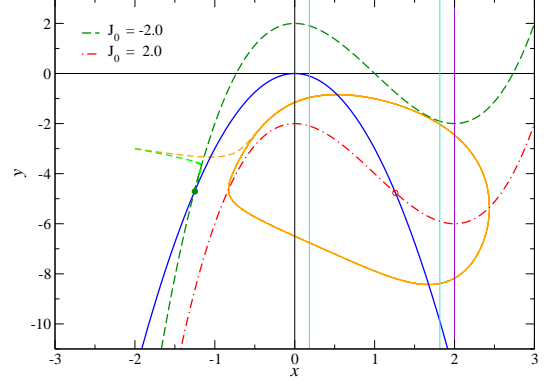
3   THE MHR NON-LINEAR ODE SYSTEM

As stated in the introduction, in Paper I and Paper II we reproduced the rich and complex behavior of GRS 1915+105 by means of a non-linear system of ODE as those used for describing quiescent and bursting signals in neuronal arrays. This approach offers the possibility of describing transitions between stable and unstable equilibrium states with the onset of limit cycles. The original Hindmarsh-Rose model (see the historic review

Figure 3. Upper plot: Fourier spectrum of the light curve of GRS 1915+105 of the *RXTE* observation on 1996 July 19 with a QPO broad peak centered at the frequency of 1.11 Hz. the yellow data are after running average smoothing to reduce the noise. Red data are those obtained after the two bandpass filtering on the fundamental and 1st harmonic feature used for deriving the QPO signal.
Lower plot: Fourier spectrum of the light curve of GRS 1915+105 of the *RXTE* observation on 1996 August 10 with a QPO broad peak centered at the frequency of 1.66 Hz. the cyan data are obtained running average smoothing to reduce the noise.

we considered also the power in the first harmonic to better approximate the true waveform. The filtered PDS spectrum of the July 19 data is shown in red in Fig. 3, showing that our method is not largely different from that used by van den Eijnden et al. (2016).

A segment of the signal obtained by the inverse Fourier transform is shown in Fig. 4. The signal structure presents an amplitude modulation applied to a carrier at the frequency of the central value of LFQPO peak like the waveform reported by van den Eijnden et al. (2016).

As already shown in Paper I, the same MHR mathematical model used for computing the light curves reported

Figure 6. Nullclines for the MHR model with $\beta = 3$ and for two J_0 values equal to -2 (green long dashed curve) and 2 (red dot-dashed curve); the solid blue curve is the parabola given by equation 4. Two phase trajectories (short dashed lines), one stable and the other describing a limit cycle, with equal initial conditions and two J_0 values are shown; green filled circle and red open circle are their equilibrium points. The turquoise vertical lines delimit the unstable equilibrium interval, and the violet line corresponds to the minima of cubic nullclines.

where the signs of the various terms were taken to have positive parameters' values. As in our previous papers we consider only the x time series that represents the X-ray photon flux of the source. Of course the solutions must be scaled both in time and amplitude to be compared with the observational data.

3.1 Nullclines, equilibrium points and stability for a constant input

In the simple case of a constant $J(t) = J_0$, an assumption that makes the model autonomous, the equilibrium conditions of equation 2, i.e. $\dot{x} = \dot{y} = 0$, are:
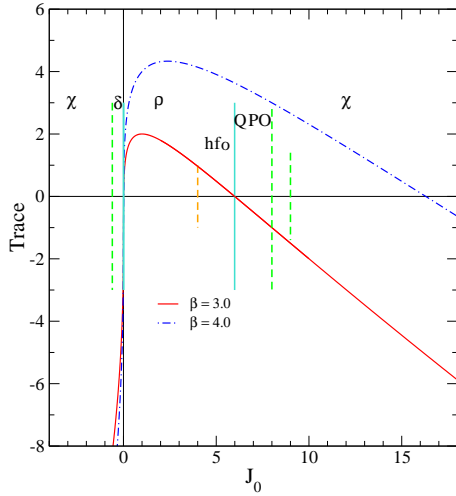
$$y = x^3 - \beta\, x^2 - J_0 \tag{3}$$

$$y = -\beta\, x^2 \tag{4}$$

The system admits only the real solution $x_* = J_0^{1/3}$, $y_* = -\beta\, J_0^{2/3}$, that corresponds to the equilibrium point. In Fig. 6 we plotted in the plane x, y the curves of equations 3 4, named nullclines, for $\beta = 3.0$ as in Paper I: they intersect at the equilibrium point, that, as we demonstrated in that paper, it results always stable for $J_0 < 0$ while there is only one unstable interval for $J_0 > 0$.

As shown in Paper I, the nature of the equilibrium depends only upon the sign of the trace of the Jacobian of the system

$$\begin{pmatrix} -3x_*^2 + 2\beta x_* & 1 \\ -2\beta x_* & -1 \end{pmatrix}$$

Figure 5. Upper plot: Light curves computed in Paper I by means of the MHR model assuming $J(t)$ of equation 6, with $C = 3.5$ and two values of $J_0 = 6.1$ (upper magenta spectrum), just higher than the transition level and 7.5 (lower indigo spectrum), both located in the stable region. Lower plot: power density spectra of these curves, shifted to separate the profiles of QPO features. The black and yellow thick curves are the Lorentzian fits to the QPO peaks.

of Hindmarsh & Cornelius 2005, and the tutorial paper Shilnikov & Kolomiets 2008) was based on three ODEs, for three dynamical variables x, y and z, involving changes on different time scales. In our previous works (Paper I; Paper II), we considered a modified system without the variable z and including an external input function of the time $J(t)$. Moreover, we adopted the simplifying assumption of taking the same quadratic coefficient in both equations, and without loss of generality, the cubic coefficient was assumed equal to 1.0. The resulting modified system, therefore, is non autonomous and includes only two ODEs that, using the same notation as in Paper I, are:

$$\begin{cases} \dot{x} = -x^3 + \beta x^2 + y + J(t) = f(x, y) \\ \dot{y} = -\beta x^2 - y = g(x, y) \end{cases} \tag{2}$$

Figure 7. Plot of the traces of the Jacobian for two values of β as function of the mean input J_0. Stable intervals (χ, QPO) for the curve relative to $\beta = 3.0$ (solid red line) are outside the long vertical turquoise solid segments, while the unstable interval (ρ) is between them. The QPO interval is indicated in the stable interval between the higher stability boundary and the local minimum of the cubic nullcline. The 'high frequency oscillation' (hfo) in the unstable interval is also indicated. Dashed vertical lines within the stable and unstable regions mark the intervals in which other variability classes and behavior are obtained as reported in the graph.

evaluated at (x_*, y_*), because the determinant is always non negative. The zeroes of the trace

$$x_{1,2} = \frac{1}{3}(\beta \pm \sqrt{\beta^2 - 3}) \qquad (5)$$

define an interval within the trace is positive and therefore the equilibrium is unstable. For $\beta = 3.0$, this unstable interval for the variable x is [0.1835, 1.8165] and is entirely contained in the interval [0.0, 2.0] that corresponds to the portion of the nullclines between the local maximum and minimum where the slope is negative, as it is easy to verify from the roots of the x derivative of equation 3. It is important to note that the instability interval on x depends only upon β but not upon J_0; thus a change of this parameter moves the location of the equilibrium point allowing transitions between stable and unstable states. However, we can relate the stability to J_0 computing the values of the trace when $J_0 = x_*^3$ varies; the resulting curves, for β, 3.0 and 4.0, are reported in Fig. 7. The two previous limits define three intervals for J_0, that we indicate as $S_1 \equiv [-\infty, 0.0061792...]$, $I \equiv [0.0061792..., 5.99382...]$ and $S_2 \equiv [5.99382..., +\infty]$. In this figure, the two turquoise vertical solid lines delimit the unstable interval I for the former value of β given above, while the equilibrium in the intervals S_1 and S_2 is stable, but the trajectories in the phase space approaching to this state are different as explained in Sect. 4.1. When J_0 varies slowly across the limits of I, transitions from stable to unstable equilibrium and *viceversa* occurs thus ruling the onset or the disappearance of the limit cycle.

Examples of stable and unstable dynamical solutions are also illustrated in Fig. 6, where two trajectories in the
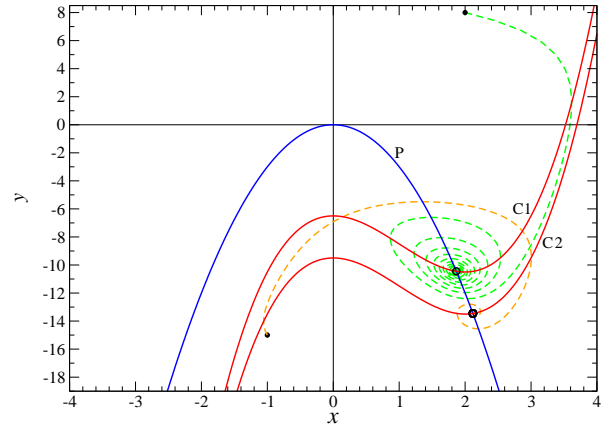
Figure 8. Nullclines for the system of equation 2 with $\beta = 3$ and for two J_0 values equal to 6.5 (red curve C1) and 9.5 (red curve C2); the blue (curve P) is the parabola given by equation 4. Stable equilibrium points are at the intersections of the parabola with the cubic lines and are marked by open circles. Two phase trajectories (dashed lines) with the different initial points, marked by black solid circles, spiralling towards the equilibrium points are also reported.

phase space corresponding to the values of $(x(t), y(t))$ of the system in equation 2 are also plotted: they start from the same initial position, $x_0 = -2.0$, $y_0 = -2.0$, but, while the one for $J_0 = -2.0$ reaches the green dashed nullcline and then moves directly towards the corresponding equilibrium point; the other (orange trajectory), computed fixing $J_0 = 2.0$, crosses the parabolic nullcline and evolves to a closed orbit (*limit cycle*) around the unstable (red open circle) equilibrium point.

4 STABLE SOLUTIONS: NUMERICAL RESULTS

Our first step was the computation of some light curves in the case of a stable equilibrium. We consider first the condition $J(t) = J_0$ without any noisy component that are useful for describing the nature of equilibrium points and the evolution of phase space trajectories; subsequently, we will present the results when random fluctuations are included in $J(t)$. In all the following calculations we will assume $\beta = 3.0$, as in Paper I. In the study of LFQPOs, the stable solutions for negative values of J_0 are not interesting and therefore we focus on the case of positive values of this parameter. Numerical computations were performed by means of a Runge-Kutta fourth order integration routine (Press et al. 2007).

4.1 Solutions without noise

The x, y trajectories in the phase space have a rather simple pattern with a transient phase, depending on the initial values, followed by a rapid approach to a steady condition (equilibrium or limit cycle). In Fig. 6 the trajectory for $J_0 = -2.0$, after the initial transient, moves very close to the cubic nullcline and then it reaches the equilibrium point. This behavior is always observed for all values of $J_0 \in S_1$. Stable

trajectories for $J_0 \in S_2$ have again an initial transient, but when the point is close to the cubic nullcline starts to describe a spiral that approximates an elliptical shape when its amplitude decreases converging to the equilibrium point. The resulting x curve tends to an exponentially damped sinusoid. A couple of such trajectories in the phase space are plotted in Fig. 8. A stable point like that of the former type is called a *sink*, while a point of the latter type is a *spiral* (see Strogatz 1994). In this figure, equilibrium points are close to the minimum of the cubic nullcline, whose coordinates are $x_m = 2\beta/3 = 2.0$ and $y_m = -4\beta^3/9 = -12.0$. There is, therefore, a rather narrow interval $[x_2, x_m]$ where the equilibrium is stable and the system describes a relatively high number of converging rounds. In Fig. 7 this interval is limited by the second turquoise and the violet vertical lines; the corresponding interval for J_0 is $S_{2*} \equiv [5.99382..., 8.0]$ and it is reported as the QPO range, although it is possible to have this feature in the adjacent intervals.

In this paper, we are interested only to equilibrium points of spiral type which can be related to the appearance of LFQPOs. The typical decay time decreases very rapidly for J_0 increasing from the stability limit to values slightly higher than x_m, thus when this parameter is between 6 and 7.5 the solution can have a rather long series of oscillations. For $J_0 > 8.0$ the phase space trajectory has a small number of cycles and for higher enough values ($\gtrsim 15.0$) the path does not encircle at all the equilibrium point. Note that also for such high J_0 value the corresponding $x_* = 2.4662..$ is quite close to x_m.

It is easy to calculate a linear approximation of the MHR system of equation 2 that gives a rather good solution in this neighbourhood:

$$\begin{cases} \dot{x} = \left(\frac{\partial f}{\partial x}\right)_m (x - x_m) + \left(\frac{\partial f}{\partial y}\right)_m (y - y_m) = y - y_m \\ \\ \dot{y} = \left(\frac{\partial g}{\partial x}\right)_m (x - x_m) + \left(\frac{\partial g}{\partial y}\right)_m (y - y_m) = \\ \\ = -\frac{4}{3}\beta^2 (x - x_m) - (y - y_m) \end{cases} \quad (6)$$

where the partial derivative are evaluated at (x_m, y_m). This linearized system is that of a damped harmonic oscillator:

$$\ddot{w} + \dot{w} + \frac{4}{3}\beta^2 w = 0 \quad (7)$$

with $w = x - x_m$. Thus the solution of the MHR model, when approaching the equilibrium point, can be well approximated by a sinusoid with an exponentially decreasing amplitude. This is seen in Fig. 8 where the trajectory for $J_0 = 6.5$ evolves to an elliptical shape converging at the equilibrium. It is interesting that the frequency of this oscillation is depending only on β and results:

$$\nu_0 = \frac{1}{2\pi}\sqrt{4\beta^2/3 - 1/4} \quad (8)$$

and the exponential decay time is equal to unity. For $\beta > 2.0$ a very good approximation (better than 2%) of this equation is $\nu_0 \approx \beta/\pi\sqrt{3}$.
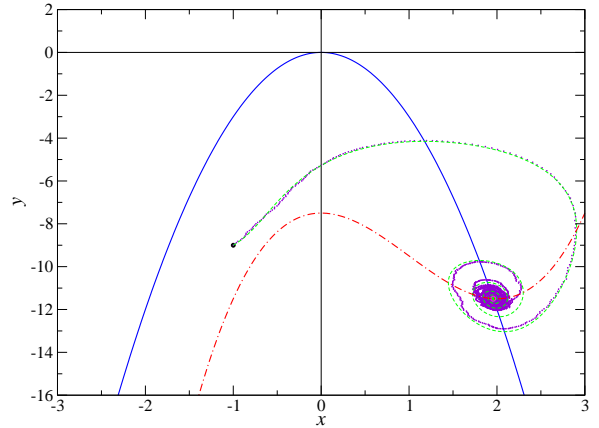
Figure 9. Numerical phase space trajectories of the MHR system with $\beta = 3$, $J_0 = 7.5$ and with a random component of amplitude $C = 6.0$ (violet dotted curve) and without the random input (green dashed curve). Red dash-dotted and solid blue curves are the cubic and the parabolic nullclines, respectively.

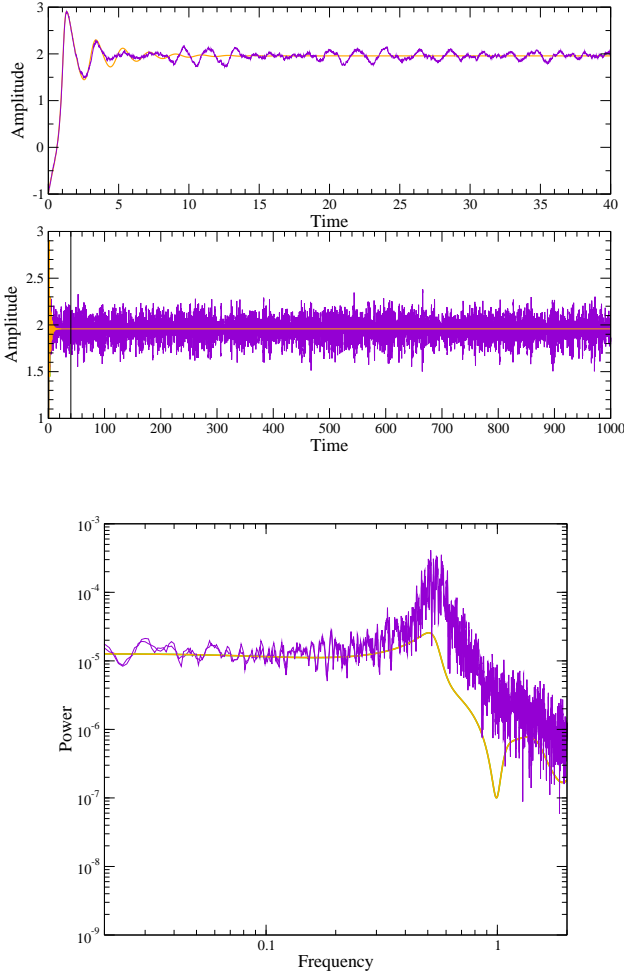### 4.2 Solutions with a random noise component

We now study the solutions when a random noise component is added to the input function

$$J(t) = J_0 + Cr(t) \quad (9)$$

where $r(t)$ is a random number with a uniform distribution in the interval $[-0.5, 0.5]$. This term is present in the equation for $\dot{x}$ and therefore it implies that the cubic nullcline in no longer stable but it is rapidly translating along the vertical axis around its mean position that is the curve corresponding to the cubic with $J(t) = J_0$.
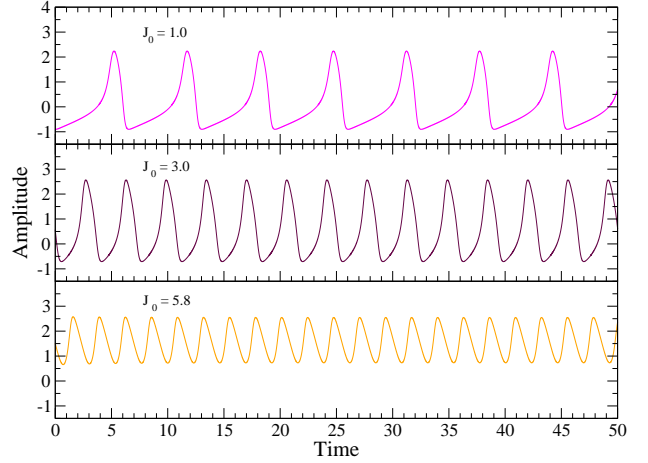
The trajectory shown in Fig. 9 was computed for $J_0 = 7.5$ and $C = 6.0$: note that in this case the random term is large enough to move the equilibrium point into the unstable region. The evolution of this trajectory, however, presents a transient in which the noise acts only as a small perturbation with respect to path in absence of noise. However, when the trajectory approaches the mean equilibrium state, it does not converges directly to this point but describes small approximately elliptical curves in its surroundings having a variable amplitude. It appears as a 'steady' situation because this oscillation continues definitively and has the aspect of a periodic signal with an amplitude modulated on a timescale ranging from about five to ten fundamental periods. The effect of large random changes of $J(t)$ appears like a weak perturbation of the trajectory because these changes act only on the derivative of x, and the corresponding variations of this variable are too small to produce a large deviation from the undisturbed path. As a consequence, the cumulative effect of these fast changes is negligible and the resulting trajectory exhibits only small deviations with respect to that corresponding to the constant J_0.

The time scale of calculated signals was chosen to have QPO frequencies close 1 Hz. The time evolution of this solution is given in the two panels of the upper plot of Fig. 10, where there is a detail of the lower plot to show the transient phase and the first segment of oscillating pattern. We also re-

Figure 11. Three light curves computed with the MHR model with $\beta = 3.0$ for different values of J_0 to show the decrease of the period and the evolution of the shape towards an approximate sinusoid.

MHR model reproduces the light curves of these unstable states with a high accuracy.
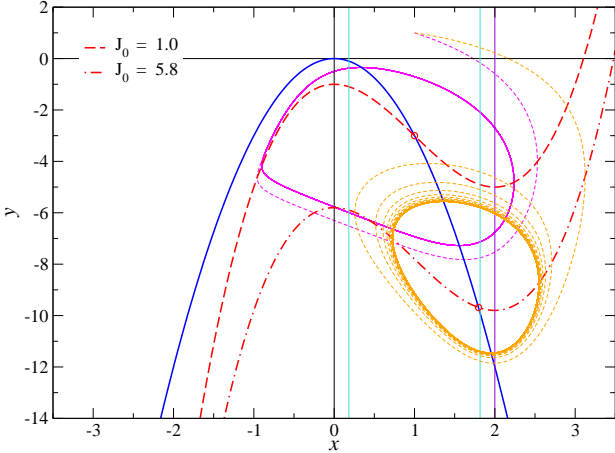
5 UNSTABLE SOLUTIONS, LIMIT CYCLE AND HIGH FREQUENCY OSCILLATIONS

For values of of J_0 within the interval $[0.0061792, 0.599382]$ the corresponding values of the equilibrium point are in the unstable interval and, as shown in Paper I, the MHR model describes a limit cycle whose light curve is like that of the ρ class (see Fig. 2). The period of the limit cycle varies regularly with J_0 according to a power law of exponent 0.5: this variation is due to the shortening of the slow leading trail making the signal shape more and more similar to a sinusoid. In Paper I we named this particular pattern 'high frequency oscillation' (shortly 'hfo') because its frequency corresponds to the highest one that one can reach increasing $J_0 \in I$ and that is slightly lower than the value estimated by means of equation 8.

These two effect are clearly visible in the three curves of limit cycles reported in Fig. 11: note, in particular, the curve for $J_0 = 5.8$, a value close the upper boundary of the unstable interval, whose profile is approximating a sinusoidal shape. The corresponding phase space trajectories are shown in Fig. 12 (only two trajectories are plotted to avoid confusion): both curves have sections in stable intervals and particularly the one with the higher J_0 is for about half cycle in the stable region. Note also that the equilibrium point is located very close to the minimum of the cubic nullcline and this confirms that equation 8 can be assumed as a valuable approximation for the 'hfo' frequency.

As seen above, the addition of a low amplitude noise introduces only small perturbations in the resulting signals, but when this amplitude increases up to a value $C = 15$ or even higher the phase space trajectory (see Fig. 13) exhibits a more complex pattern with large separated annular patterns, implying a low frequency modulation. A short segment of the light curve is in the upper plot in Fig. 14, where

Figure 10. Upper plot: in the upper panel there is the initial segment of the numerical time solutions for the x variable of the system of equation 2 with $\beta = 3$, $J_0 = 7.5$ and a random component amplitude $C = 6.0$ (violet dotted curve) and without the random input (orange thick curve); in the lower panel there is a longer light curve with the same parameters' values to show that the pattern remains stable, the vertical line limits in the interval shown in the upper plot. Lower plot: Fourier PDS of the quasi-periodic oscillation after a 3 point running average, the lower orange curve is the PDS of the signal without noise shown in in the same figure. Note that the peak frequencies are the same, but the height of the latter spectrum is much lower than the one of QPO signal.

ported the solution without the random noise to make clear the different behavior of the resulting curves when this component is considered. The lower plot reports the corresponding PDS, where a LFQPO feature, remarkably similar to the one observed in GRS 1915+105 (see Fig. 3), confirming t hat in these conditions the MHR model can originate this phenomenon. The resulting light curve is like those shown in the upper plot of Fig. 5 and therefore it is also remarkably similar to that derived from the filtered data. This similarity reduces the PDS degeneracy, i.e. the fact that different types of signal have analogous PDS, and confirms that the
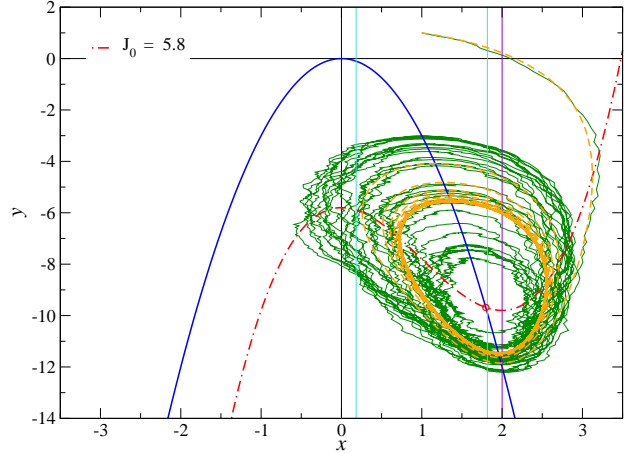
Figure 12. Phase space plot to show the nullclines (red and blue curves) and the trajectories (dashed lines) of two curves in Fig. 11. Turquoise vertical lines delimit the unstable interval and the violet line indicates the coordinate of the cubic nullcline minimum.


Figure 13. Phase space plot to show the nullclines (red dot-dashed and solid blue curves) and the trajectories of an MHR result for $J_0 = 5.8$ without (orange dashed line) and with (dark green line) a noise component with $C = 20$.. Turquoise vertical lines delimit the unstable interval and the violet line indicates the minimum coordinate of the cubic nullcline.

the amplitude modulation is evident. In the lower plot of the same figure we report the PDS of the this signal exibiting a prominent broad peak again very similar to the LFQPO feature in Fig. 3. The solid black line is PDS of the 'hfo' without noise. The main peak and its harmonics are more evident after a light smoothing (turquoise data in the same figure) and its central frequency is slightly lower than that of 'hfo' without noise. As a further remark we underline that the structure of the noisy phase space trajectory in Fig. 13 is recalling the solutions of the Lorenz model (Lorenz 1963) and therefore it suggests that the chaotic behavior found in some light curves of GRS 1915+105 (Misra et al. 2006) can be related to the same processes described by the MHR model, that is not properly a chaotic deterministic system, but a noise perturbed limit cycle.

6   NOISE LEVEL AND LFQPO INTENSITY

Our results indicate that the occurrence of LFQPOs is dependent upon the presence of a noisy component: in other conditions, in fact, solutions exhibit a 'hfo' or converge spiralling toward the equilibrium point according to the value of J_0, lower or higher the threshold stability, respectively. We verified this connection performing some numerical calculations with different choices of parameters and, in the following, we show the results of nine cases for three choices of J_0 and three of C. The former parameter was taken equal to 5.7 in the I 'hfo' interval, to 6.5, that is in S_{2*}, and to 8.0, so that the equilibrium point coincides with the local minimum of the cubic nullcline. The three values of C are 1.0, 5.0 and 9.0.

The resulting PDS are given in the three panels in Fig. 15. The top panel shows the PDSs for the 'hfo' state with increasing added noise: the spectrum of the lowest noise data exhibits a harmonic series of narrow peaks about two orders of magnitude higher than the noise amplitude. A lower and lower number of harmonics appears also when

the noise increases but the central frequency and width remain stable to the 'hfo' value, that is equal to 0.41 in the units corresponding to those adopted for the time. For J_0 high enough to move the system in the stable region and a QPO feature is always present in the PDS, but with only one or two harmonics. Its central frequency decreases slightly for increasing noise from 0.51 to 0.48, in any case higher by about 20% than in the previous case. A further increase of J_0 moves the equilibrium point at the cubic local minimum and the PDS continues to present the QPO peak but it appears mild and with the only the first harmonic barely detectable; its central frequency is stable at 0.545, as expected from equation 8.

## 7   THE ORIGIN OF LFQPOS IN THE MHR MODEL

As shown in the introduction, the MHR model reproduces well light curves of several variability classes according to the values of the single parameter J_0, which controls transitions from stable to unstable equilibrium. In the latter states the system describes a limit cycle whose period decreases for increasing J_0 and the spike profiles change to a more and more symmetric shape that approximates a sinusoid with a short and constant period, here named 'high frequency oscillations'. A further increase of J_0 produces a transition to the second stable region thus we expect a signal evolving to a steady level. In Sect. 4 we discussed the nature of the equilibrium points and showed that they are of type *sink* of of type *spiral* according that the value of J_0 is in S_1 or S_2, respectively. In the latter case the x curve presents a number of oscillations before to reach the final value. Fast fluctuations of the $J(t)$ generally act on the phase space trajectories as small perturbations with respect to the one corresponding to the mean value J_0. For values close to the upper boundary of the unstable interval I, the system excite 'hfo' modes
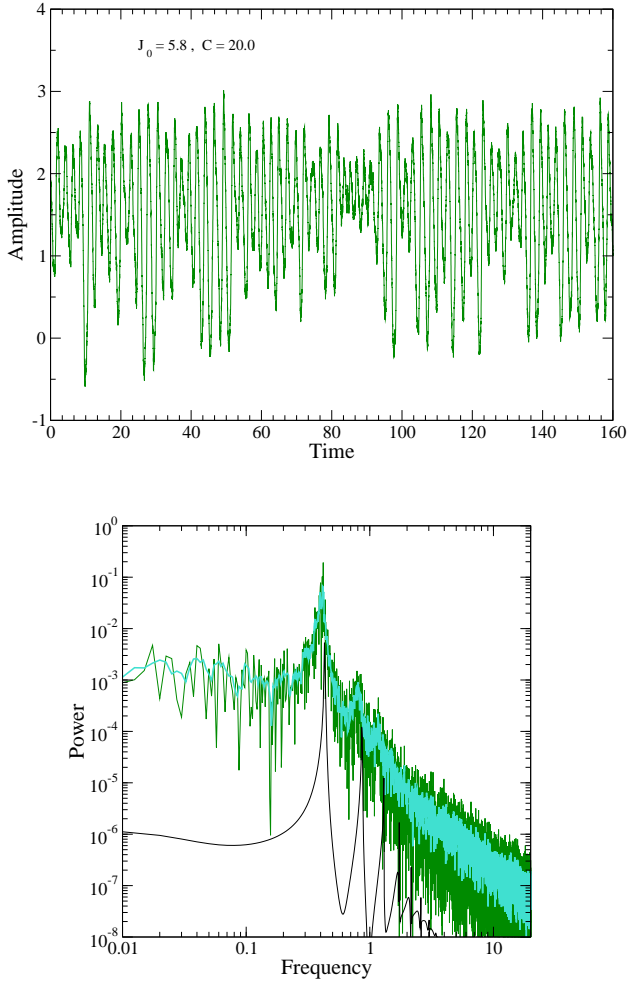
Figure 14. Upper plot: Light curve computed with the MHR model with $\beta = 3.0$ and $J_0 = 5.8$ and a large noise component ($C = 20$). Note the asymmetry of the signal with the noise fluctuations greater in the lower part of the curve than in the upper one. Lower plot: Fourier PDS of the signal in the upper panel (dark green data) showing a well evident broad peak and three harmonics; these features are more apparent after a running average over 5 points (turquoise data). The black spectrum is that of the signal without noise.

with an amplitude modulation on longer time scales. The corresponding PDS shows a broad feature, typical of LFQPOs frequently found in BHCs, like GRS 1915+105. When J_0 values are above the stability threshold the equilibrium point remains always in the stable region, and LFQPOs are also present if the x coordinate of this point is lower than or close to the minimum of the cubic nullcline. These results allow us to favor an "intrinsic" hypothesis on the origin of LFQPOs in an accretion disc essentially related to the same mechanism responsible of the spiking limit cycle and occurring for J_0 values close to transition between the unstable and the stable region.

The role of random fluctuations, that could be due to plasma turbulence in the disc, in establishing LFQPOs was already noticed in a paper by Maccarone et al. (2011), who computed the bispectrum of some observations of GRS
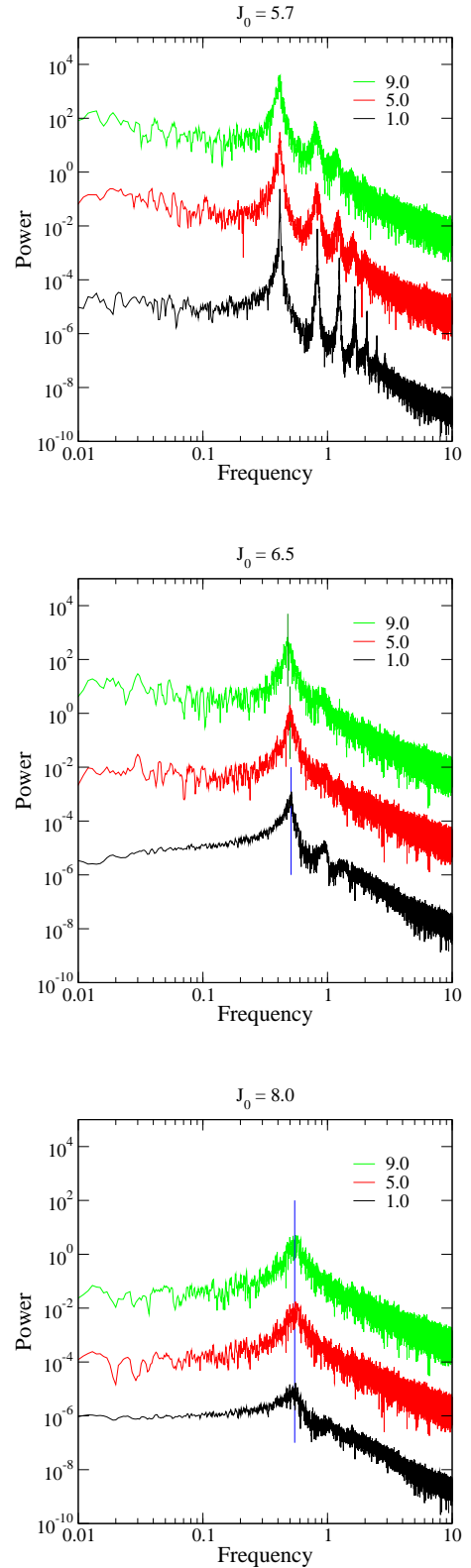
Figure 15. Top plot: PDS computed by means of MHR model for $\beta = 3.0$ and $J_0 = 5.7$ and three different noise levels; spectra were vertically shifted to avoid confusion.
Central plot: PDS computed for $J_0 = 6.5$; vertical lines mark the central frequencies of LFQPO peaks.
Bottom plot: PDS computed for $J_0 = 8.0$.

1915+105 and found a correlation between LFQPOs and the variations of the noise component. This tool provides the possibility of discriminating among the various variability modes producing similar PDS and Maccarone et al. (2011) concluded that "the variability is caused by a reservoir of energy being drained by a noise component ... and a quasi-periodical component, while in the brighter part of the χ state, the variability is consistent with a white noise input spectrum driving a damped harmonic oscillator with a non-linear restoring force." MHR results are in agreement with this finding and confirm the relevance of the noise, in particular we found that small deviations from the decaying trajectory perturb it towards a different path which converges again to the equilibrium until another small deviation restores a similar condition. Then the noise is like a stabilizing factor for the LFQPO and their frequency is limited in a rather narrow interval close to the one of the corresponding oscillator at the local minimum of the cubic as shown in Sect. 4.

The correlations of LFQPO frequency with the photon energy of the source luminosity are useful for addressing possible relationships with the MHR model parameters. For example, according equation 8, these correlations would imply that the parameter β must be linear depending on the photon energy.

It is important to point out that our results does not exclude geometric models for LFQPOs, particularly in some sources which do not exhibit the same complex variability of GRS 1915+105. These models can naturally account for some phenomena as the modulation of the iron line energy as a function of QPO phase (see, for instance, Ingram et al. 2016; Nathan et al. 2019). The present version of the MHR model is only focused on the time stucture of the brightness changes and does not include any energy dependence of the emission and, particularly, the properties of the iron line. We stress that it should be considered as a simple tool approximating the non-linear instability in accretion discs which produces the large variety of light curves, as those observed in GRS 1915+105. It may have, however, a heuristic content because can help the understanding of some features and details, like the spike profiles or the LFQPO signal structure.

8   CONCLUSION

In Paper I; Paper II we proposed the non linear mathematical MHR model, containing only a small number of parameters, whose solutions reproduce several different classes of light curves of GRS 1915+105 , and describe well the transition from stables to bursting states. An interesting finding of this model was that it is also able to describe the occurrence of LFQPOs as a consequence of a transition from an unstable to a stable equilibrium. In the present paper we studied in detail the nature of this transition and compare the model results with some observational data.

The major findings of the present work are related to the fact that the stable equilibrium points where LFQPOs are present is of the *spiral* type. Moreover, we found that for values of the driving parameter J_0 within the interval S_{2*}, the equilibrium point lies between the stability threshold and the local minimum of the cubic nullcline. In this condition the phase space trajectories converge to the equilibrium point

describing a tight spiral around it, that corresponds to an oscillating pattern in the model light curve. It follows that the PSDs are very similar to the observed ones with a broad Lorentzian feature and, occasionally, one or two harmonics. The general structure of model light curves is also like the observed ones after a filtering in the peak range.

Another important finding is that the fluctuations of J_0 play a role in stabilizing LFQPOs: without noise the phase space trajectory converges to the equilibrium and light curves are like a damped oscillation, while random displacements can move the trajectory towards outer positions from which a new path approaching to equilibrium follows. Without noise the occurrence of long duration LFQPOs would not be possible. This result confirms the bispectral analysis of some light curves of GRS 1915+105 by Maccarone et al. (2011) who pointed out the noise relevance in the process responsible of LFQPOs. The possibility of noise-induced quasi-periodic oscillation in the original HR model including three ODEs was also considered by Ryashko & Slepukhina (2017), confirming thus the relevance of the random fluctuations although in different conditions. Turbulence in accretion discs is important because it can provide a driving mechanism also for HFQPOs and can produce the 3:2 twin peak feature, as demonstrated by the numerical model recently developed by Ortega-Rodríguez et al. (2020). In Sect. 3 we derived a simple linear approximation of the MHR model that was used for estimating the central frequency of the Lorentzian peak in a narrow interval around the local minimum of the cubic nullcline that was found to be depending only on the parameter β. More generally, one could expect that this frequency is determined by the shape of equilibrium track near the minimum and, if this curve can be derived from a physical stability calculations as made, for instance by Watarai & Mineshige (2001) (see Paper II), one could relate the observed LFQPO data to some parameters of the accretion disc.

These results suggest a possible explanation why many BHCs exhibit LFQPOs but not the large variety of light curve profiles as those of GRS 1915+105. In fact, it would be sufficient that the values of the equivalent J_0 in these sources remain for all the time in the range corresponding to an equilibrium point close or just above the boundary between the unstable interval of 'hfo' and spiral trajectories. An interesting property worthwhile of investigation is if such a condition can be related to their disc sizes which for many BHCs are estimated much lower than GRS 1915+105 (Remillard & McClintock 2006).

The present results confirm that MHR model is a simple and efficient approximation for describing the instabilities in an accretion disc and predicting a large variety of light curves that are originated in this type of physical processes. Using this model we also showed that the origin of LFQPOs can be explained by the same instability, but for values of the input parameter in a range higher than the unstable interval. There are, however, some relevant topics to further study: the most important is to complete the physical interpretation of the model and the association of the mathematical variables with physical quantities of the accretion disc. This association requires numerical calculations of equilibrium states and an analysis of their stability using hydrodynamic codes. It is also possible that in this way one will open the possibility of adding the variable energy and

of achieving a more complete mathematical modelling of the source behaviour in different bands.

DATA AVAILABILITY

Data used in this paper are available in a repository and can be accessed via link https://heasarc.gsfc.nasa.gov/cgi-bin/W3Browse/w3browse.pl.

REFERENCES

Belloni T., Klein-Wolt M., Méndez M., van der Klis M., van Paradijs J., 2000, A&A, 355, 271
Casella P., Belloni T., Homan J., Stella L., 2004, A&A, 426, 587
Casella P., Belloni T., Stella L., 2005, ApJ, 629, 403
Castro-Tirado A. J., Brandt S., Lund N., 1992, IAUC, 5590, 2
Chakrabarti S. K., Molteni D., 1993, ApJ, 417, 671
Chen X., Taam R. E., 1992, MNRAS, 255, 51
Chen X., Taam R. E., 1995, ApJ, 441, 354
Fender R., Belloni T., 2004, ARA&A, 42, 317
Hindmarsh J. L., Cornelius P., 2005, 2005, BURSTING: The Genesis of Rhythm in the Nervous System. S. Coombes & P.C. Bressloff eds
Ingram A., van der Klis M., 2015, MNRAS, 446, 3516
Ingram A., Done C., Fragile P. C., 2009, MNRAS, 397, L101
Ingram A., van der Klis M., Middleton M., Done C., Altamirano D., Heil L., Uttley P., Axelsson M., 2016, MNRAS, 461, 1967
Lasota J., 2016, Astrophysics of Black Holes - From fundamental aspects to latest developments. Springer-Verlag Berlin Heidelberg, doi:10.1007/978-3-662-52859-4
Lorenz E. N., 1963, Journal of Atmospheric Sciences, 20, 130
Maccarone T. J., Uttley P., van der Klis M., Wijnands R. A. D., Coppi P. S., 2011, MNRAS, 413, 1819
Marcel G., et al., 2020, arXiv e-prints, p. arXiv:2005.10359
Markwardt C. B., Swank J. H., Taam R. E., 1999, ApJ, 513, L37
Massaro E. Capitanio F., Feroci M., Mineo T., Ardito A., Ricciardi P., 2020a, MNRAS, in press, (Paper I)
Massaro E. Capitanio F., Feroci M., Mineo T., Ardito A., Ricciardi P., 2020b, MNRAS, in press, (Paper II)
Misra R., Harikrishnan K. P., Ambika G., Kembhavi A. K., 2006, ApJ, 643, 1114
Morgan E. H., Remillard R. A., Greiner J., 1997, ApJ, 482, 993
Motta S. E., 2016, Astronomische Nachrichten, 337, 398
Muno M. P., Morgan E. H., Remillard R. A., 1999, ApJ, 527, 321
Nathan E., Ingram A., Homan J., Uttley P., 2019, Proc. X-ray Astronomy 2019 - Current Challenges and new frontiers in the Next Decade, Bologna 2019, Contr. 5500,
Ortega-Rodríguez M., Solís-Sánchez H., Álvarez-García L., Dodero-Rojas E., 2020, MNRAS, 492, 1755
Paul B., Agrawal P. C., Rao A. R., Vahia M. N., Yadav J. S., Marar T. M. K., Seetha S., Kasturirangan K., 1997, A&A, 320, L37
Press W. H., Teukolsky S. ., Vetterling W. T., Flannery B. P., 2007, Numerical Recipes: The Art of Scientific Computing, 3 edn. Cambridge University Press
Remillard R. A., McClintock J. E., 2006, ARA&A, 44, 49
Rodriguez J., Durouchoux P., Mirabel I. F., Ueda Y., Tagger M., Yamaoka K., 2002, A&A, 386, 271
Ryashko L., Slepukhina E., 2017, Phys. Rev. E, 96, 032212
Shilnikov A., Kolomiets M., 2008, International Journal of Bifurcation and Chaos, 18, 2141
Strogatz S. H., 1994, Nonlinear Dynamics and Chaos. Westview Perseus Books Group, Reading MA
Szuszkiewicz E., Miller J. C., 1998, MNRAS, 298, 888
Taam R. E., Lin D. N. C., 1984, ApJ, 287, 761
Taam R. E., Chen X., Swank J. H., 1997, ApJ, 485, L83
Tagger M., Pellat R., 1999, A&A, 349, 1003
Varnière P., Tagger M., Rodriguez J., 2012, A&A, 545, A40
Watarai K.-Y., Mineshige S., 2001, PASJ, 53, 915
Wijnands R., Homan J., van der Klis M., 1999, ApJ, 526, L33
Yan S.-P., Ding G.-Q., Wang N., Qu J.-L., Song L.-M., 2013, Monthly Notices of the Royal Astronomical Society, 434, 59
van den Eijnden J., Ingram A., Uttley P., 2016, MNRAS, 458, 3655
van der Klis M., 1989, ARA&A, 27, 517

This paper has been typeset from a TeX/LaTeX file prepared by the author.